

Auto-calibration and real-time external parameter correction for stereo digital image correlation

Zhilong Su^a, Lei Lu^b, Shuai Dong^c, Fujun Yang^a, Xiaoyuan He^{a,*}

^a School of Civil Engineering, Southeast University, Nanjing 210096, China

^b College of Information Science and Engineering, Henan University of Technology, Zhengzhou 450001, China

^c School of Civil Engineering, Changsha University of Science and Technology, Changsha, 410114, China

ARTICLE INFO

Keywords:

Auto-calibration
Bundle adjustment
External parameter correction
Stereo digital image correlation

ABSTRACT

Calibrating stereo digital image correlation (stereo-DIC) is crucial for 3D deformation measurements. Existing stereo-DIC calibration methods mainly rely on a well-made planar target with additional specific coding to perform pre-calibration. In this paper, a new method is proposed to calibrate a stereo-DIC system automatically with feature correspondences in an unconstrained scene. In contrast to traditional methods, the proposed method is scale-independent and does not require assumptions such as planarity. More importantly, it is capable of correcting disturbed external parameters in real time. With inverse depth parameterization, a stereo-DIC system can be effectively calibrated by a carefully designed bundle adjustment framework. Subsequently, a fast correction strategy based on massive-point subset tracking is derived to recalibrate the disturbed stereo-DIC system. The proposed method overcomes the predicament of reduced measurement accuracy due to the unavoidable disturbance of external parameters in dynamic deformation measurements. Experiments were conducted to verify the effectiveness of the proposed method.

1. Introduction

Stereo digital image correlation (stereo-DIC) technology is increasingly used to characterize the behavior of materials and structures undergoing deformations. Stereo-DIC is stereo computer vision-based, full-field, and non-contact deformation measurement technology, and it mainly relies on accurate system calibration to reduce reconstruction errors in order to obtain reliable deformation fields [1]. The technology often works well in controllable environments (such as laboratories), because known targets can be used conveniently, and external conditions, such as illumination, vibration, and temperature, are well controlled to maintain system reliability. With stereo-DIC technology gradually moving towards real applications, however, several problems caused by uncontrolled environments have severely limited its applicability in most practical fields. One of the most important challenges involves performing reliable system calibration in uncontrolled environments. Because artificial targets are difficult to apply in an unconstrained scene; moreover, inevitable environmental vibration can affect the stability of system calibration [2]. Calibrating a stereo-DIC system refers to estimating the internal and external parameters of its stereo vision system. According to the pinhole model [3], internal parameters comprise the intrinsic geometry and optical characteristics of its camera component, including the focal lengths, principal point, and distortion factors. External

parameters refer to the extrinsic geometry of the stereo camera system, including its relative rotation and translation. Considerable research has resulted in the development of many calibration methods using known 3D objects [4], planar targets [5–10], unknown space scenes [11–14], etc.

Planar-target-based calibration techniques are widely used in stereo-DIC owing to their accuracy and operability in controlled environments [15,16]. Existing methods typically aim to increase the accuracy of parameters by using a specially designed pattern and/or calibration algorithm. A planar target with a marker chessboard pattern was proposed by Chen et al. for calibrating a stereo camera rig using a frame optimization strategy and a bundle adjustment (BA) method [8]. Cui et al. reported a calibration method that minimizes the residual error in 3D space rather than on the image plane to obtain precise parameters [17]. Jia et al. proposed an accuracy calibration method that determines the internal parameters by compensating for perpendicularity and then estimates external parameters using centroid-based optimization [18]. More recently, a planar coding pattern was designed by Li et al. to calibrate a stereo vision system using a BA model [19]. However, planar-target-based calibration methods require the size of the pattern to match the size of the field of view (FOV). As such calibration is difficult and expensive in uncontrolled environments. This limits the applications of these methods.

* Corresponding author.

E-mail address: mmhxy@seu.edu.cn (X. He).

Calibrating a stereo-DIC system from an unknown space scene is also attractive owing to the advantage of recovering all calibration parameters without using any known pattern [11]. Much research has been devoted to this approach, starting in computer vision, and more recently in the DIC community. Liu et al. proposed a stereo calibration method that decomposes external parameters from epipolar geometry determined by point correspondences [12]. However, their method requires calibrating the cameras in advance, and its accuracy is relatively low for stereo-DIC measurements. Herrera et al. proposed a homography-based method to recover all calibration parameters from an unknown planar scene [13]. Guan et al. further developed this method to give closed-form initial values for stereo geometry under the planar assumption, before estimating the calibration parameters using an optimization algorithm [14]. However, the planar hypothesis means that the method cannot be used directly for non-planar deformation measurements. More recently, Shao et al. calibrated a single-lens 3D video extensometer to measure strain according to a speckle-based calibration algorithm [20]. However, this method is highly dependent on good speckle quality and reliable initial value transfer for speckle matching; in addition, it is a local intensity-based method and, as such, requires a relatively stable illumination environment. Furthermore, the speckle must occupy a large part of the FOV.

In this paper, we propose a generative method for calibrating stereo-DIC systems to overcome the limitations of existing methods. The proposed method not only automatically estimates all calibration parameters from unconstrained scene images directly, it can also be used to quickly correct disturbed external parameters, effectively reducing errors in 3D deformation measurements. Based on inverse depth representation and an efficient radial distortion model, a robust BA framework is built on feature correspondences by minimizing the re-projection residual in the normalized image domain. To construct correspondences for fast external parameter correction, a highly concurrent subset tracking scheme based on massive feature point initialization is given. Then, a real-time auto-correction strategy for external parameters is derived from the proposed BA framework. Finally, the proposed method is validated in two 3D deformation measurement experiments. To our knowledge, there are few real-time extrinsic geometry correction algorithms for stereo-DIC.

This paper is organized as follows. The proposed BA framework for stereo-DIC calibration and the auto-correction strategy for external parameters are presented in Section 2. The experimental results are given to verify the proposed method in Section 3. The advantages and potential applications for the proposed method are discussed in Section 4. We conclude the paper in Section 5.

2. Principle

An overview of the proposed calibration method for stereo-DIC is illustrated in Fig. 1. Based on feature correspondences, a geometric BA is carefully designed to calibrate a stereo-DIC system reliably using a group of stereo images throughout the measurement process rather than an artificial calibration target. According to the calibrated results, a real-time external parameter correction strategy is developed from the BA framework for dynamic deformation measurements. Details are described in the following subsections.

2.1. Bundle adjustment of stereo-DIC calibration

The BA framework is designed with a radial distortion model to jointly estimate the calibration parameters of the stereo-DIC system. We accomplish this by introducing the inverse depth representation of back-projection and measuring the residual of projection in the normalized image domain. This helps to reduce the complexity of the cost function and regularize the scales of the variables to cope with features over a wide range of depths. Consequently, the BA can be robustly built on the unconstrained scene with enough precision for defor-

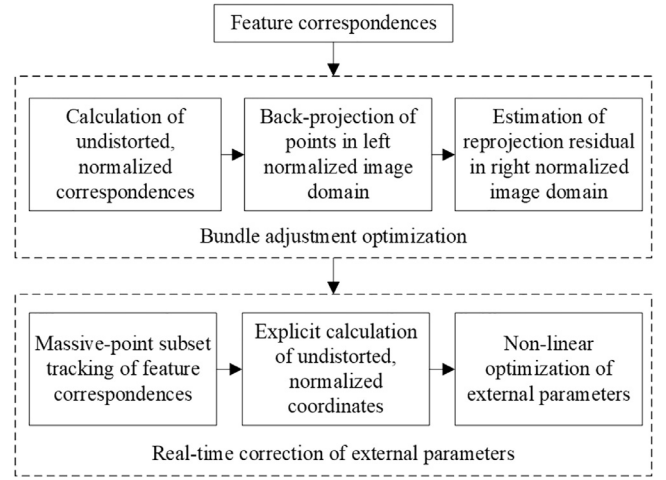


Fig. 1. Overview of the proposed auto-calibration method for a stereo-DIC system.

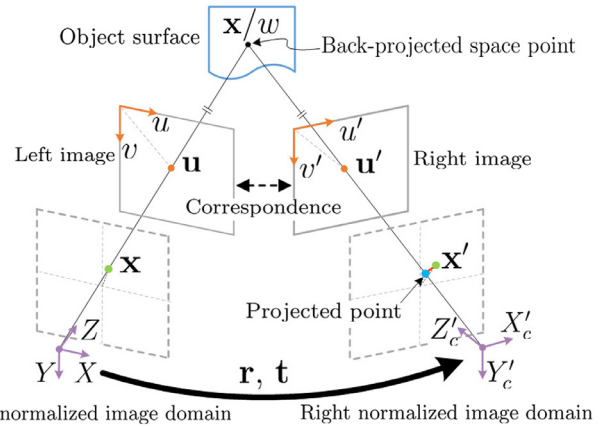


Fig. 2. Triangulation geometry used in our BA for stereo-DIC calibration.

mation measurements. To introduce our BA, we begin with the radial distortion. Conventional distortion models used in stereo-DIC calibration map the points from an undistorted image onto a distorted image [5,15,20,21]. However, describing the back-projection in an analytic form is not straightforward because it is difficult to obtain an exact analytic inverse function. Instead, we adopt a distorted-to-undistorted radial distortion model to build our BA in a new way, avoiding any loss to its analytic form, which is essential for non-linear optimization. Because this distortion model maps the points from a distorted image onto an undistorted image directly, we found that it offers improved efficiency for both BA optimization and 3D reconstruction, as well as mitigating accuracy loss due to distortion rectification.

We follow the reasonable assumption that aligns the world coordinate system to the left camera coordinate frame. The geometry used in this study is depicted in Fig. 2. Let \mathbf{u} be the left feature in a given correspondence with homogeneous coordinates. With the radial distortion model, its undistorted position in a normalized image domain is analytically calculated by

$$\mathbf{x} = K^{-1} \mathbf{u} D(K^{-1} \mathbf{u}), \quad (1)$$

$$D(\cdot) = 1 + k_1 \|\cdot\|^2 + k_2 \|\cdot\|^4, \quad (2)$$

where K is the intrinsic matrix of the camera (here, we suppose that the skew factor is zero), and $D(\cdot)$ is the radial distortion function. The back-projection of feature \mathbf{u} to its space coordinate is thus parameterized by its inverse depth w with an analytic form of \mathbf{x}/w . Then, the back-

projected point is mapped into the right normalized image domain by a projection function \mathcal{P} as follows:

$$\mathcal{P}(\mathbf{x}; \mathbf{r}, \mathbf{t}, w) = \langle \mathcal{R}(\mathbf{r}) \mathbf{x}(K, k_1, k_2) + w\mathbf{t} \rangle, \quad (3)$$

where \mathbf{r} and \mathbf{t} respectively denote the relative rotation and translation from the left camera to right camera, $\mathcal{R}(\cdot)$ is the Rodrigues formula that transforms the rotation vector to a matrix, and $\langle \cdot \rangle$ is the normalization operator from $(x, y, z)^T$ to $(x/z, y/z, 1)^T$.

As shown in Fig. 2, the discrepancy between the projected point and the undistorted coordinate \mathbf{x}' of the right feature \mathbf{u}' in the normalized image, which is calculated with the same method as that in Eq. (1), is used as a residual metric for the proposed BA. For all extracted feature correspondences $\{\mathbf{u}_{ij} \leftrightarrow \mathbf{u}'_{ij}\}$, the proposed BA framework can be formulated by minimizing the residuals of all the projected coordinates as

$$\underset{\mathbf{K}, \mathbf{r}, \mathbf{t}, \mathbf{w}}{\operatorname{argmin}} \sum_{j=1}^m \sum_{i=1}^n \mathcal{L}(\mathbf{x}'_{ij}(K', k'_1, k'_2) - \mathcal{P}(\mathbf{x}_{ij}(K, k_1, k_2); \mathbf{r}, \mathbf{t}, w_{ij})), \quad (4)$$

where m is the number of stereo images, n is the number of correspondences in each stereo image, $\mathcal{L}(\cdot)$ indicates a loss function, \mathbf{K} is the set of internal parameters $\{f_x, f_y, c_x, c_y, k_1, k_2; f'_x, f'_y, c'_x, c'_y, k'_1, k'_2\}$, and \mathbf{w} is the set of inverse depths $\{w_{ij}\}$. Because of feature correspondences, we use the Levenberg–Marquardt algorithm [22,23] to minimize the pseudo-Huber loss function in [24], instead of the squared loss, for robustness to possible outliers. It should be noted that the proposed model also works for system calibration using a single image pair. However, the experiments described in Section 3.1 show that using a stereo image sequence is better for two reasons: it makes the proposed BA more robust to noisy image data, reducing parameter estimation errors; and it enhances the capacity of the triangulation model, defined by the calibration parameters, to cope with out-of-plane deformations, such that the 3D shape at each measurement step can be recovered optimally. Consequently, the system is more precise.

The well-known SURF method [25] is employed to build feature correspondences $\{\mathbf{u}_{ij} \leftrightarrow \mathbf{u}'_{ij}\}$. The SURF algorithm is not only capable of fast detection of features with sub-pixel location, it also sensitive to both blob-like and corner-like features. This ensures that our BA can use a set of full-FOV distributed feature correspondences from the scene for stereo-DIC applications. This is critical to obtain accurate distortion factors and principle points. In addition, a robust local similarity invariant representation makes the external parameter correction strategy fast, as explained in the next section.

For the initial values of the proposed BA framework, the focal lengths can be initialized as $f_x = \frac{W}{S_x} f$ and $f_y = \frac{H}{S_y} f$, where f is the physical focal length, (S_x, S_y) is the sensor size, and (W, H) is the image width and height. The principle point can be initialized as the image center $(\frac{W}{2}, \frac{H}{2})$. The radial distortion factors are initialized to zero. The initial external parameters can be estimated in two ways: according to the initial arrangement of the cameras, the relative rotation and translation can be initialized as $(0, \theta, 0)^T$ and $(B, 0, 0)^T$, where θ and B are the pre-estimations for the stereo angle and width of the baseline, respectively; or they can be determined with a fast linear decomposition algorithm [12], which can be performed conveniently after the feature correspondences are constructed. The latter is recommended because it gives an initial estimation that is closer to the optimal parameters to speed up the optimization. The initialization for inverse depths is heuristic. For flat calibration scenes, the inverse depths can be initialized with a unified value determined from the work distance. If the features used are detected from an unconstrained scene, it is recommended to assign a random inverse depth between 0.01 and 1.0 to each feature point.

2.2. Real-time auto-correction of external parameters

In some practical applications for stereo-DIC, environment vibration is unavoidable while measuring deformations. This can change the external geometry of a calibrated stereo-DIC system, leading to large

measurement errors. Therefore, disturbed external parameters should be corrected with enough accuracy to ensure the precision of deformation measurements. However, we cannot interrupt the consecutive measurement process to recalibrate the stereo camera using the planar target. Therefore, we here propose a real-time auto-correction strategy to overcome the disadvantages of existing methods for high-precision deformation measurements in dynamic and/or uncontrollable environments. We found that using the current image pair suffices to perform a reliable external parameter correction during the current measurement step, provided that the system has been calibrated by our BA. This is for two reasons: the calibrated data gives a good initialization for both external parameters and inverse depths; and cameras with prime lenses allow us to re-estimate disturbed external parameters with the pre-calibrated, fixed internal parameters [9,12,16].

Because the correction should be performed during the deformation calculation, it is rather time-consuming to re-detect and re-match SURF features in the deformed image sequence. Fortunately, every SURF point that we used has a salient intensity feature and good intensity gradient response within its neighborhood. Therefore, a high-precision subset registration scheme with the inverse compositional Gauss–Newton (IC-GN) algorithm [26–28] is suitable for tracking the accurate position of each feature in a sequence of deformed images. Considering the continuity of deformation, the matched SURF features can be used as the initial values for the IC-GN algorithm to achieve fast feature matching. In contrast to the conventional subset matching method where the initial value is transferred from a single seed point [26,27], feature point initialized subset matching is more reliable and essentially concurrent, because it is performed independently at each point. Thus, it is possible to construct the correspondences with a real-time massive-point matching scheme. The image on the left in Fig. 2 at the initial stage is given as a reference image. The details of the proposed correction strategy are described as follows:

Step 1: Key point preparation. Because the SURF features we obtained in the reference image have sub-pixel coordinates, we truncate their coordinates to obtain a set of key points with integer coordinates to track correspondences. In this way, the reference subset for each key point can be obtained directly from the reference image, avoiding superfluous intensity interpolation due to the sub-pixel position.

Step 2: Massive-point tracking. We want to compute the displacement for each key point to track the feature correspondences. Displacement refers to the position difference of a key point in the reference and current stage. Here, it is computed by using subset matching, which includes temporal matching in left image and stereo matching in right image. The pipeline is illustrated with the forward solid arrows in Fig. 3. The IC-GN algorithm with a first-order shape function is recommended for subset matching. The critical operation in this step is to select the image patch centered on the matched SURF feature as the target subset for each key point. This is implemented by resampling the current image using biquintic spline interpolation. In fact, this also gives the initial guess for the displacement that is to be estimated. Let f and g be the intensity at position (i, j) in the reference and target subsets, respectively, and \mathbf{W} be the shape function. The optimal displacement of a key point is refined by solving the normalized inverse compositional least-squares problem with the Gauss–Newton method:

$$\underset{\Delta \mathbf{p}}{\operatorname{argmin}} \sum_{(i,j)} \left[\frac{f(\mathbf{W}(i, j; \Delta \mathbf{p})) - \bar{f}}{\sqrt{\sum_{(i,j)} [f(i, j) - \bar{f}]^2}} - \frac{g(\mathbf{W}(i, j; \mathbf{p})) - \bar{g}}{\sqrt{\sum_{(i,j)} [g(i, j) - \bar{g}]^2}} \right]^2, \quad (5)$$

where \bar{f} , \bar{g} are the mean intensity value of the two subsets, \mathbf{p} is the shape parameters with six elements (viz., the displacement and its gradients), and $\Delta \mathbf{p}$ is the shape parameter update being estimated. The details for Eq. (5) can be found in [27]. The advantage of the inverse compositional form objective lies in the evaluation of the steepest descent image on the reference subset, which remains constant across iterations. Because both temporal and stereo matching can be simultaneously initialized

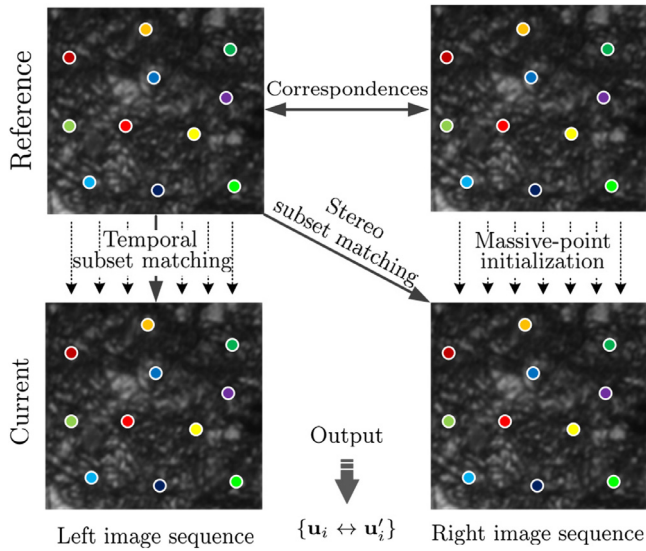


Fig. 3. Massive-point concurrent subset matching scheme for a stereo image. The matched points are rendered with the same color.

with the tracked SURF features (schematically shown as dashed arrows in Fig. 3), this step can be sped up on a GPU platform [29] to achieve massive-point matching with real-time performance. Finally, a set of new correspondences $\{u_i \leftrightarrow u'_i\}$ is extracted from the stereo image at the current stage.

Step 3: External parameter correction. The output correspondences in Step 2 inherit the matching relationship from the initially matched SURF correspondences (the matched points are marked by the same color in Fig. 3). They can be directly used to recalculate the external geometry of the stereo-DIC system. With the calibrated cameras in Section 2.1, the feature correspondences are explicitly transformed to their normalized positions via Eq. (1) to obtain a set of fixed, normalized correspondences $\{x_i \leftrightarrow x'_i\}$ in advance. Therefore, a concise non-linear model for external parameter correction can be derived from the proposed BA framework as follows:

$$\underset{\mathbf{r}, \mathbf{t}, \mathbf{w}}{\operatorname{argmin}} \sum_{i=1}^n \delta_i \mathcal{L}(x'_i - \langle \mathcal{R}(\mathbf{r}) \mathbf{x}_i + w_i \mathbf{t} \rangle), \quad (6)$$

where $\delta_i = 1$ if the i -th correspondence is tracked successfully; otherwise, it is 0. The initial values for Eq. (6) can adopt the results of the previous calibration step, such that the non-linear equation can be solved more efficiently by explicit using the sparse Schur complement. The corrected external parameters can then be used to recover the object shape at the current stage. 3D displacement at each reconstructed point is ultimately estimated by comparison to the reference coordinates with a common scale in the common coordinate system.

Because we assume the object shape is recovered in a reference frame aligned to the left camera frame, 3D reconstruction can only be performed locally using the corrected external parameters if the pose of the left camera is not stable. To recover 3D shapes in a common coordinate system, it is necessary to determine the relative rotation and translation between the common and current reference frame. A common rule of thumb is to select a set of reference points on a stable, separate frame in the FOV. To select the reference points, multi-scale detectors, such as SURF, are recommended, because the extracted scale-invariant points will be more robust to possible blur and illumination variation. Another practice involves setting some fixed targets, such as circular or cross markers, on a distinct reference object. The artificial targets can be tracked stably with high positioning accuracy. This method is more useful for controlled reference objects, such as a vibration table. Because reference points are assumed to be fixed, a set of linear equations with nine unknowns (six for rotation and three for translation) can be estab-

Table 1
Results of calibrated internal parameters.

Parameter	Our BA method		Chessboard method	
	left	right	left	right
f_x	2401.75	2403.51	2495.29	2498.34
f_y	2398.45	2397.26	2497.51	2487.14
c_x	632.80	630.92	590.44	597.15
c_y	500.74	501.10	473.44	475.86
k_1	0.1845	0.1800	-0.1701	-0.1616
k_2	-0.3901	-0.4560	0.0016	0.0019

Table 2
Results of calibrated external parameters.

Parameter	Our BA method	Chessboard method	DLD method
$\mathbf{r}^T(^{\circ})$	(-0.04, 48.52, -0.11)	(0.45, 45.77, -0.19)	(1.09, 51.16, 1.29)
\mathbf{t}^T	(1.00, 0.01, -0.43)	(1.00, 0.01, -0.44)	(1.00, 0.01, -0.58)

lished according to their spatial positions in the common and current reference frames. The transformation from the current reference frame to the common coordinate system can be easily determined by solving the linear equations. Finally, the locally reconstructed object points can be mapped into the common coordinate system for displacement estimation.

3. Experimental results

In this section, the performance of the proposed BA framework is discussed based on a real static experiment, described in Section 3.1. The performance of the auto-correction strategy for external parameters is described in Section 3.2. The precision of stereo-DIC systems calibrated by our method was compared to that of existing methods, by adopting the same program module for performing the DIC algorithm [26,30] and strain calculation [31] to ensure that the non-calibration errors were identical.

3.1. Static deformation measurement

A single-lens stereo-DIC system (with a light path similar to the device in [20]) was used in this experiment to measure the deformation of a simply supported plate subjected to out-of-plane load. The designed stereo angle of our device is 48° . The focal length is 12 mm and the resolution is 1280×1024 pixels. The work distance is 135 mm and the size of FOV is $35 \text{ mm} \times 55 \text{ mm}$. The specimen was made of Inconel 718 alloy and was $150 \text{ mm} \times 30 \text{ mm} \times 3 \text{ mm}$ in size. Its top surface was painted with a speckle pattern. A strain gage was adhered to the bottom surface at mid-span. The experimental setup is shown in Fig. 4(a). To compare the results, the system was calibrated with the following methods: chessboard method (9×6 corners with 3 mm spacing), direct linear decomposition (DLD) [12], and the proposed BA.

3.1.0.1. Calibration results. Our BA used five stereo images (two non-deformed and three deformed image pairs), and 799 SURF correspondences were selected in each stereo image. The correspondences in a non-deformed stereo image are shown in Fig. 4(b). For chessboard calibration, 50 target poses were captured to obtain stable calibration parameters. The DLD method used the internal parameters estimated by the chessboard and the correspondences in BA calibration. The calibrated internal parameters for the proposed method and the chessboard method are listed in Table 1. The external parameters produced by the three methods are listed in Table 2. The relative translation vectors were normalized because the true-to-scales of translations obtained by our method and the DLD method were unknown.

Table 1 shows that the results of both methods are consistent except for the radial distortion factors. The main reason for this is that

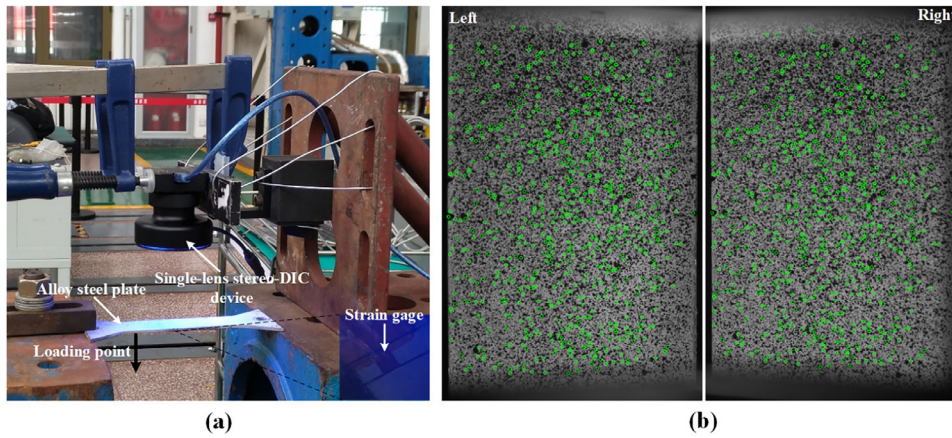


Fig. 4. (a) Experimental setup and (b) matched SURF feature correspondences.

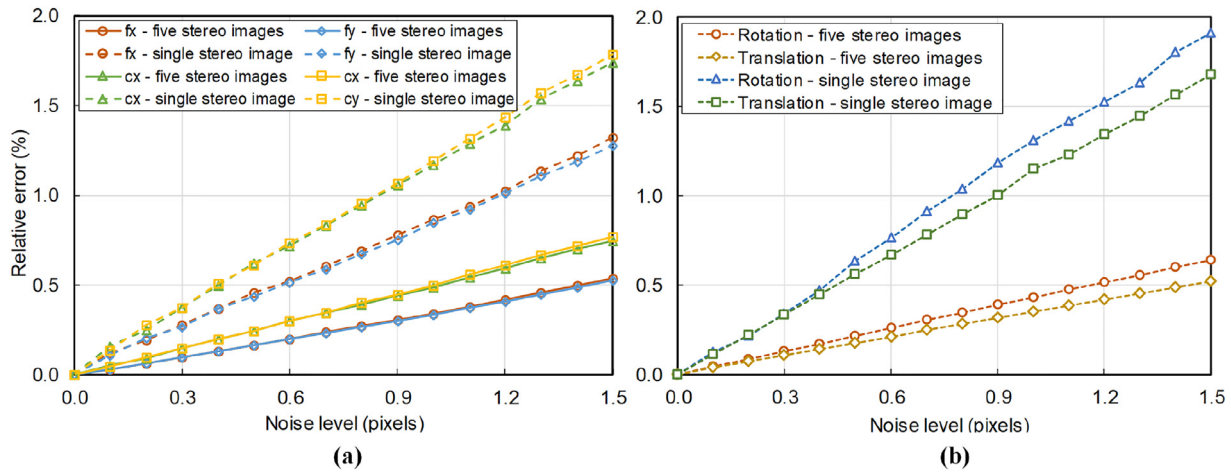


Fig. 5. Calibration parameter errors with increasing image noise.

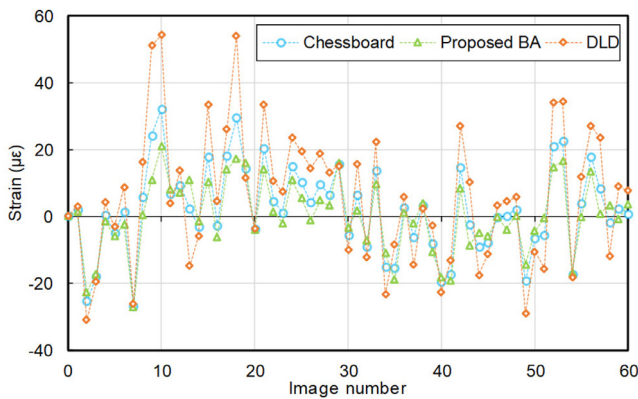


Fig. 6. Results of static error evaluation.

the employed radial distortion models differed, as mentioned above. Table 2 shows that the rotation vector optimized by our BA is closer to the designed angle vector $(0^\circ, 48^\circ, 0^\circ)^T$. In terms of re-projection, the error of our method is 0.02 pixels, which is better than that of the chessboard method (0.08 pixels), and much better than that of the DLD method (0.38 pixels).

3.1.0.2. Performance with respect to the noise level. We investigated the performance with respect to the noise level using a stereo image sequence and a single image pair. The image sequence was composed by the foregoing five stereo images; the single image pair was the first one

in the sequence. Similarly, 799 correspondences were constructed for each stereo image. We used the previous BA calibrated parameters as a ground truth. Gaussian noise with zero mean was added to each feature. The standard deviation (SD) was varied from 0.1 pixels to 1.5 pixels to simulate noise conditions. For each noise level, we performed 200 independent calibration trials. The parameters estimated each trial were compared to the ground truth. We computed the relative error for each internal parameter and the two-norm-based relative error for r and t . The average results are shown in Fig. 5. As expected, all errors increased linearly with the noise level added to the feature points. (The error for each distortion parameter is not shown, but has the same property.) By comparing errors in both internal and external parameters, we can see that using an image sequence helps to improve the anti-noise performance of the proposed BA framework significantly.

3.1.0.3. Performance test on strain measurement. The proposed method was first validated by evaluating static errors on 60 non-loaded images, and then by conducting 10-step loading measurements. We measured the strain data using the three calibrated stereo-DIC systems. The subset size was 31×31 pixels, and the window size for strain computation was 9×9 points. A small rectangular region with a size close to that of the gage was selected according to pre-drawn positioning lines. We estimated the average strain values in this small region and compared these to the standard values. The static errors are illustrated in Fig. 6. The measured strain values and their differences relative to the standard values are shown in Fig. 7. Comparisons of both static and measurement errors are listed in Table 3. As expected, the differences among measurement systems with different calibration parameters are systematic.

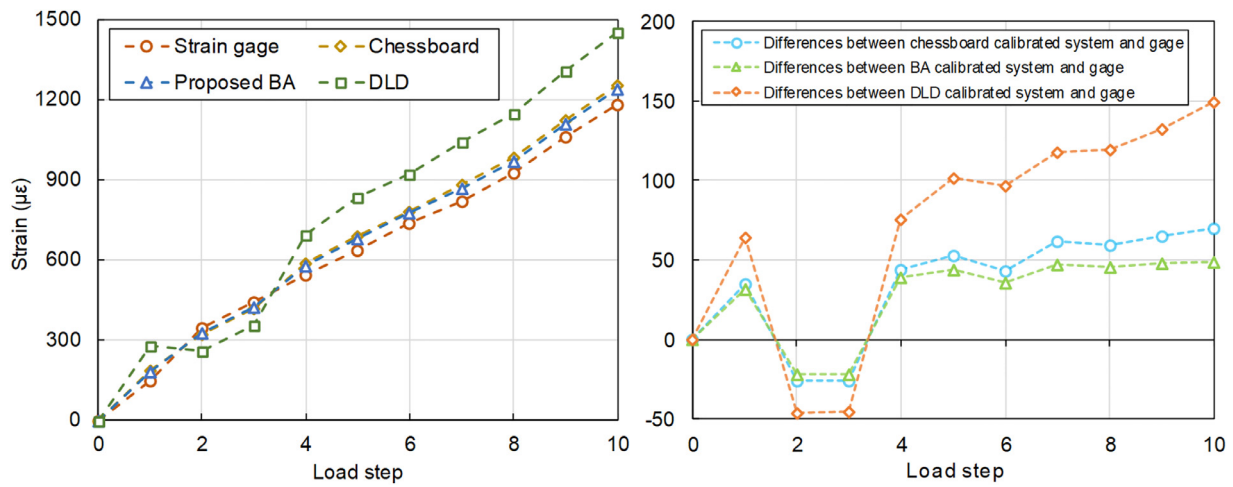


Fig. 7. (a) Measured strain values and (b) differences in measurement results between the strain gage and stereo-DIC systems calibrated by the proposed BA, chessboard, and DLD methods.

Table 3

Comparisons of static and measurement errors ($\mu\epsilon$).

Calibration method	Static error		Measurement error	
	error range	SD	maximum difference	SD
BA	[-27, 21]	10.5	48.9	26.4
Chessboard	[-27, 32]	13.0	69.6	33.7
DLD	[-35, 55]	29.8	149.8	66.3

For static error evaluation, the mean errors for the systems calibrated by the proposed BA, chessboard, and DLD methods were $1.5 \mu\epsilon$, $2.0 \mu\epsilon$, and $14.8 \mu\epsilon$, respectively. For the proposed BA and the commonly used chessboard calibration, we can see that static errors of the systems calibrated by both methods are coincident and stable; a comparison of these measurement errors shows that the former is slightly more accurate than the latter. By contrast, both static and measurement errors with the DLD-calibrated system were rather large in this well-controlled experiment (the maximum strain value is approximately $1183 \mu\epsilon$). Additionally, Fig. 7(b) illustrates the errors of the system calibrated by the DLD method, which increase considerably with the load after the third load step. The main reason for this is that only a single stereo image was used for external parameter calibration. Consequently, the error caused by out-of-plane deformation could not be restrained effectively. Thus, the proposed BA is a feasible and trustworthy calibration method for stereo-DIC.

3.2. Validation of external parameter correction strategy

The performance with respect to the matching error was validated, followed by a dynamic experiment to validate its effectiveness with on-line deformation measurements.

3.2.1. Performance with respect to the feature matching error

Before evaluating the performance with respect to the matching error, the stability of the proposed external parameter correction method was investigated. The non-loaded image sequence in Section 3.1 was used in this test. Again, 799 correspondences were constructed from the first stereo image and tracked in subsequent stereo images, where the subset size was 21×21 pixels. The external parameters were estimated according to the tracked correspondences and then compared to the BA-produced initial values in Table 2. The two-norm-based relative errors for rotation and translation vectors were measured. The results are shown in Fig. 8(a). The mean errors of the estimated relative ro-

tation and translation vector were 1.80×10^{-3} with SD 6.73×10^{-4} and 1.21×10^{-3} with SD 8.73×10^{-4} , respectively.

To examine the influence of the matching error, Gaussian noise with zero mean was added to the feature correspondences in the first non-loaded stereo image. We varied the SD from 0.1 pixels to 5.0 pixels to simulate the matching error. For each error level, 200 independent trials were performed. The estimated parameters were compared to those with no additional errors. The average relative errors were computed and shown in Fig. 8(b). The errors with external parameter estimation increase linearly with the matching error level, and the error in relative translation is lower than that in relative rotation.

3.2.2. Performance evaluation with dynamic strain measurements

A shock test with a steel box girder was conducted. The actual goal of this test is to measure the dynamic strain response. Here, we used it to evaluate the proposed external parameter correction method by comparing the stereo-DIC measured results to those recorded by the strain gage. The span of the girder was 1500 mm and the size of the cross profile was $100 \text{ mm} \times 50 \text{ mm} \times 5 \text{ mm}$. The girder was loaded by a mechanical shock system composed of a lifting motor and a mass block. A strain gage was adhered at the lower edge on the reverse side of the girder. The stereo-DIC system comprised two high-speed cameras (FASTCAM SA3, 50 mm lens) with a resolution of 1024×1024 pixels. The camera frame rate was set to 1000 Hz to capture images during the lifting impact test. The size of the region of interest was $250 \text{ mm} \times 100 \text{ mm}$. The setup for the experiment is shown in Fig. 9(a). The deformation data was computed by processing the image data on-line. Considering the transmission delay incurred by downloading images from both cameras to the computer's memory, the system estimated the strain data every 100 ms from the moment at maximum impact load. For that, 18 stereo images were finally downloaded and used. Similar to the test described in Section 3.1, the average strain in a small region was calculated for comparison with the values of the strain gage. A total of 882 point correspondences were used in this experiment. Massive-point tracking was executed on a GPU platform (NVIDIA Quadro M2000M), where the size of the subset was 41×41 pixels. The proposed correction algorithm was implemented using C++ language and executed on a laptop (Intel(R) Xeon(R) CPU with an E3-1535M 2.90 GHz processor and 8 GB RAM).

The stereo-DIC was calibrated with the following schemes: (1) planar target calibration with a chessboard (11×8 corners, 25 mm spacing), which could only be performed before the loading; (2) one-shot calibration using the proposed BA described in Section 2.1, which was also executed before loading; and (3) based on the calibrated results from Scheme 2, external parameters were corrected before every strain cal-

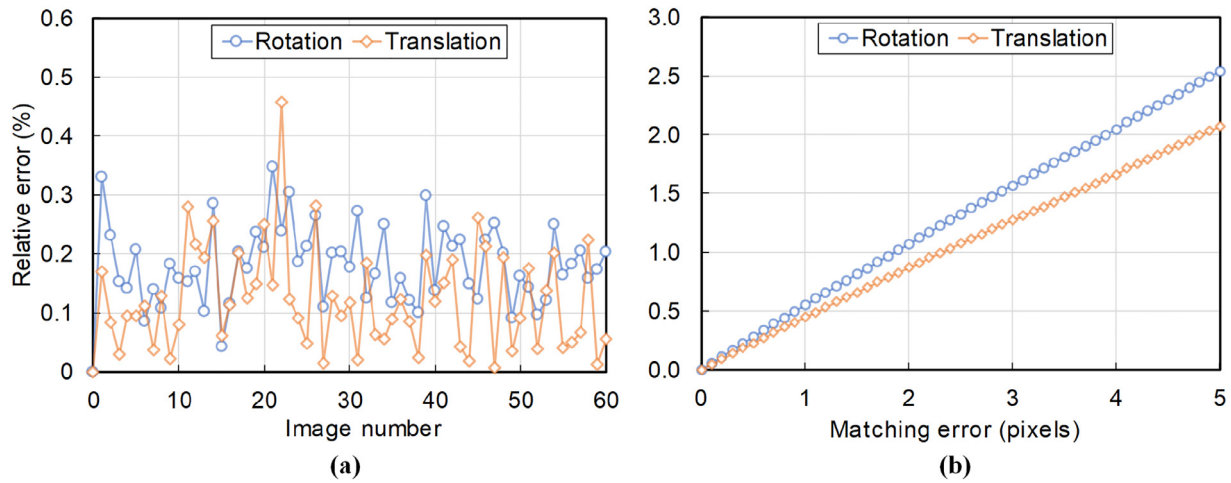


Fig. 8. (a) Results of stability evaluation and (b) errors for rotation and translation as a result of increasing the matching error.

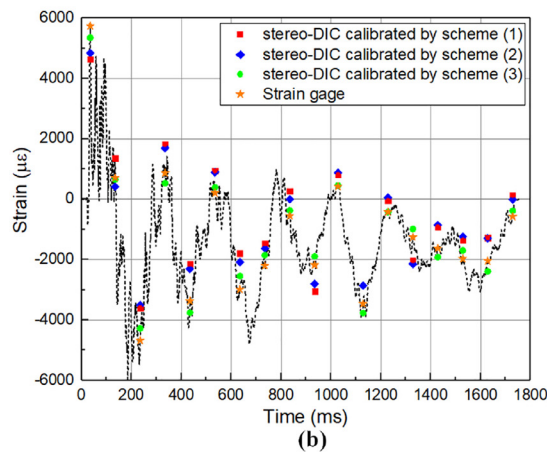
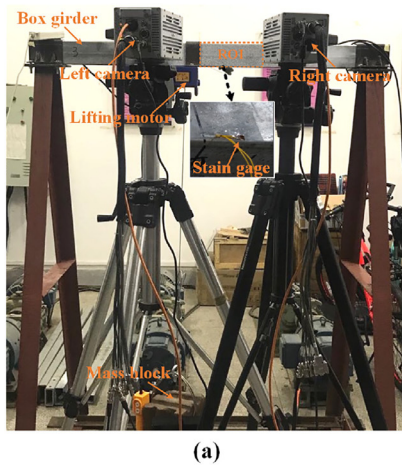


Fig. 9. (a) Experimental setup and (b) measured strain values. The dashed curve is the complete strain time history recorded by the gage. Several values of the strain gage are highlighted with yellow symbols for comparison. (For interpretation of the references to colour in this figure legend, the reader is referred to the web version of this article.)

calibration step using the proposed strategy. Fig. 9(b) shows the measured results. Compared to the values of strain gage, the maximum absolute errors of Schemes 1 and 2 were $1081.4 \mu\epsilon$ with an SD of $620.9 \mu\epsilon$ and $994.6 \mu\epsilon$ with an SD of $601.5 \mu\epsilon$, respectively. However, the maximum absolute error of Scheme 3 was only $378.5 \mu\epsilon$ with an SD of $264.2 \mu\epsilon$. In addition, the evaluated static errors before impact loading were all less than $200.0 \mu\epsilon$. These results show that the measurement errors of a stereo-DIC with corrected external parameters are clearly below those of systems calibrated by one-shot calibration schemes and closer to static errors. A lower SD implies that the measurement system calibrated by Scheme 3 is more stable. The main reason for the difference in accuracy is that the impact load caused ground vibrations, especially when loading began—when the load amplitude was at its maximum (the strain curve in Fig. 9(b) also shows this phenomenon). The ground vibration disturbed the calibrated external geometry, resulting in large errors in strain measurements when the external parameters were not corrected. The efficiency can be verified by the average time cost for all correction stages. The average time spent for both temporal and stereo matching was approximately 8 ms; each correction step was completed in an average of 36 ms. The correction strategy was executed at a speed of approximately 23 Hz on our test laptop, which is sufficient for on-line stereo-DIC measurements.

The experiment demonstrates that the proposed strategy significantly reduces measurement errors incurred by unstable external parameters of a stereo-DIC system with real-time speed. Meanwhile, it

illustrates the necessity of external parameter correction for dynamic deformation measurements.

4. Discussion

The calibration of stereo-DIC has certain peculiarities compared to ordinary stereo vision calibration, which is determined by the specialty of its applications. Especially for applications in industrial and engineering fields, there are several inherent attributes, such as a large structure size, successive measurements, unavoidable environment vibration, etc., lead to existing calibration methods cannot be effectively applied to stereo-DIC technology. This is because, on the one hand, large-scale measurements lead to several problems for existing stereo calibration methods of stereo-DIC, such as operational difficulties, poor accuracy, and high costs. On the other hand, the cameras of the stereo-DIC system often have a wide baseline. As such, camera components cannot be connected rigidly in real applications and calibrated external parameters can be disturbed during measurements due to environment vibrations or improper operation. To address these problems, an auto-calibration and real-time extrinsic geometry correction framework for stereo-DIC was proposed. The method is advantageous for the following reasons: it offers automatic calibration of a stereo-DIC system with high accuracy; it is robust to noise and mismatched correspondences; it does not depend on the real size of the measured object; and it offers real-time and accurate external geometry correction.

For the proposed auto-calibration method, it should be noted that the true-to-scale of the body being measured cannot be recovered directly.

However, it can be determined easily using a scale bar or target with a known size when necessary. The proposed real-time external parameter correction method was verified in experiments, which demonstrated its effectiveness at reducing measurement errors with dynamic measurements. Indeed, the proposed system may be more useful for long-term dynamic measurements. Owing to the ample volume of image data for such measurements, the cost of transferring and storing all the source data is often expensive. On-line computation is thus desirable to capture deformation data of interest for reducing storage loads. However, environmental vibrations can affect the stability of the calibrated external geometry, leading to considerable measurement errors and even invalid deformation data. By applying the proposed real-time correction method, however, measurement errors caused by unstable external parameters will be reduced significantly, ensuring the validity of the data. In addition, the computational cost incurred by corrections is quite low, and will not affect the efficiency of on-line computations. This improves the practicability of stereo-DIC technology for high-precision dynamic measurements.

There are potential stereo-DIC applications for the proposed method. For example, it could be used to calibrate a multi-camera stereo-DIC system automatically [16,32]. It is difficult to use existing methods, such as a planar pattern, to calibrate a multi-camera system pair-wisely, and precise calibrations cannot easily be ensured. However, the proposed method could calibrate each pair of cameras efficiently and optimize the external parameters of the sub-systems jointly to improve the overall calibration accuracy. As another potential application, the proposed method could be employed to calibrate a microscopic stereo-DIC system [33]. The cost of small but highly precise calibration targets is very high, and planar targets need be controlled by precise instruments during calibration. Therefore, the proposed method could also facilitate the development of microscopic stereo-DIC technology.

5. Conclusion

This paper proposed a new approach based on geometric triangulation to calibrate a stereo-DIC system for deformation measurements. The proposed auto-calibrating BA framework was built on inverse depth parameterized back-projection in analytic form to model and process any feature in an unconstrained scene. Compared to other calibration methods, the proposed BA framework accurately calibrates a stereo-DIC system from the scene of a measurement FOV directly. We demonstrated the feasibility of correcting disturbed external parameters in real time by simplifying our BA to a concise form. We achieved this by explicitly mapping the correspondences tracked by the proposed concurrent matching scheme to their undistorted, normalized positions. Finally, we evaluated the performance of the proposed calibration method by conducting two real stereo-DIC experiments. Our results indicate that, with the proposed approach, stereo-DIC has the potential to be applied more widely, such as for large structure measurements, structural health monitoring, dynamic tests, and engineering and biological material measurements.

Funding

National Natural Science Foundation of China (NSFC) (11532005, 11772092, 11827801, 61705060).

References

- Becker T, Splitthof K, Siebert T, Kletting P. Error estimations of 3d digital image correlation measurements. *Proc SPIE* 2006;6341. doi:10.1117/12.695277. 6341 – 6341 – 6
- Ramos T, Furtado A, Eslami S, Alves S, Rodrigues H, Arede A, et al. 2D and 3d digital image correlation in civil engineering-measurements in a masonry wall. *Procedia Eng* 2015;114:215–22. doi:10.1016/j.proeng.2015.08.061.
- Sturm P, Ramalingam S, Tardif J-P, Gasparini S, Barreto J. Camera models and fundamental concepts used in geometric computer vision. *Found Trends Comput Graph Vis* 2011;6(1–2):1–183. doi:10.1561/06000000023.
- Faugeras OD, Toscani G. The calibration problem for stereo. In: *IEEE Conference on Computer Vision and Pattern Recognition*. IEEE; 1986. p. 15–20.
- Zhang Z. A flexible new technique for camera calibration. *IEEE Trans Pattern Anal Mach Intell* 2000;22(11):1330–4. doi:10.1109/34.888718.
- Vo MN, Wang Z, Luu L, Ma J. Advanced geometric camera calibration for machine vision. *Opt Eng* 2011;50. doi:10.1117/1.3647521. 50 – 50 – 4
- Yin Y, Peng X, Li A, Liu X, Gao BZ. Calibration of fringe projection profilometry with bundle adjustment strategy. *Opt Lett* 2012;37(4):542–4. doi:10.1364/OL.37.000542.
- Chen J, Benzeroual K, Allison RS. Calibration for high-definition camera rigs with marker chessboard. In: *2012 IEEE Computer Society Conference on Computer Vision and Pattern Recognition Workshops*. IEEE; 2012. p. 29–36. doi:10.1109/CVPRW.2012.6238905.
- Liu Z, Yin Y, Liu S, Chen X. Extrinsic parameter calibration of stereo vision sensors using spot laser projector. *Appl Opt* 2016;55(25):7098–105. doi:10.1364/AO.55.007098.
- Rathnayaka P, Baek S-H, Park S-Y. An efficient calibration method for a stereo camera system with heterogeneous lenses using an embedded checkerboard pattern. *J Sens* 2017;2017:12.
- Schmidt J. *3-D Reconstruction and stereo self calibration for augmented reality*. CiteSeer; 2006.
- Liu R, Zhang H, Liu M, Xia X, Hu T. Stereo cameras self-calibration based on sift. In: *2009 International Conference on Measuring Technology and Mechatronics Automation*. IEEE; 2009. p. 352–5. doi:10.1109/ICMTMA.2009.338.
- Herrera D, Kannala CJ, Heikkila J. Forget the checkerboard: Practical self-calibration using a planar scene. In: *2016 IEEE Winter Conference on Applications of Computer Vision*. IEEE; 2016. p. 1–9. doi:10.1109/WACV.2016.7477641.
- Guan B, Shang Y, Yu Q. Planar self-calibration for stereo cameras with radial distortion. *Appl Opt* 2017;56(33):9257–67. doi:10.1364/AO.56.009257.
- Sutton MA, Orteu J-J, Schreier H. *Image correlation for shape, motion and deformation measurements: basic concepts, theory and applications*. 1st. Springer; 2009. ISBN 0387787461, 9780387787466.
- Dong S, Yu S, Huang Z, Song S, Shao X, Kang X, et al. Target-based calibration method for multifields of view measurement using multiple stereo digital image correlation systems. *Opt Eng* 2017;56. doi:10.1117/1.OE.56.12.124102. 56 – 56 – 8
- Cui Y, Zhou F, Wang Y, Liu L, Gao H. Precise calibration of binocular vision system used for vision measurement. *Opt Express* 2014;22(8):9134–49. doi:10.1364/OE.22.009134.
- Jia Z, Yang J, Liu W, Wang F, Liu Y, Wang L, et al. Improved camera calibration method based on perpendicularity compensation for binocular stereo vision measurement system. *Opt Express* 2015;23(12):15205–23. doi:10.1364/OE.23.015205.
- Li W, Shan S, Liu H. High-precision method of binocular camera calibration with a distortion model. *Appl Opt* 2017;56(8):2368–77. doi:10.1364/AO.56.002368.
- Shao X, Eisa MM, Chen Z, Dong S, He X. Self-calibration single-lens 3d video extensometer for high-accuracy and real-time strain measurement. *Opt Express* 2016;24(26):30124–38. doi:10.1364/OE.24.030124.
- Ravn O, Andersen NA, Sørensen AT. Auto-calibration in automation systems using vision. In: *Yoshikawa T, Miyazaki F, editors. Experimental Robotics III*. Springer Berlin Heidelberg; 1994. p. 206–18. ISBN 978-3-540-39355-9.
- Levenberg K. A method for the solution of certain non-linear problems in least squares. *Quart Appl Math* 1944;2:164–8. doi:10.1090/qam/10666.
- Marquardt D. An algorithm for least-squares estimation of nonlinear parameters. *Journal of the Society for Industrial and Applied Mathematics* 1963;11(2):431–41. doi:10.1137/0111030.
- Hartley R, Zisserman A. *Multiple view geometry in computer vision*. 2nd Edition. Cambridge University; 2003. ISBN 0521540518.
- Bay H, Ess A, Tuytelaars T, Gool LV. Speeded-up robust features (surf). *Comput Vision Image Understand* 2008;110(3):346–59. doi:10.1016/j.cviu.2007.09.014.
- Pan B, Li K, Tong W. Fast, robust and accurate digital image correlation calculation without redundant computations. *Exp Mech* 2013;53(7):1277–89. doi:10.1007/s11340-013-9717-6.
- Gao Y, Cheng T, Su Y, Xu X, Zhang Y, Zhang Q. High-efficiency and high-accuracy digital image correlation for three-dimensional measurement. *Opt Lasers Eng* 2015;65:73–80. doi:10.1016/j.optlaseng.2014.05.013.
- Su Y, Zhang Q, Xu X, Gao Z, Wu S. Interpolation bias for the inverse compositional gauss-newton algorithm in digital image correlation. *Opt Lasers Eng* 2018;100:267–78. doi:10.1016/j.optlaseng.2017.09.013.
- Wang T, Kemao Q. Parallel computing in experimental mechanics and optical measurement: a review (ii). *Opt Lasers Eng* 2018;104:181–91. doi:10.1016/j.optlaseng.2017.06.002.
- Chen L, Treece GM, Lindop JE, Gee AH, Prager RW. A quality-guided displacement tracking algorithm for ultrasonic elasticity imaging. *Med Image Anal* 2009;13(2):286–96. doi:10.1016/j.media.2008.10.007.
- Pan B, Xie H, Guo Z, Hua T. Full-field strain measurement using a two-dimensional savitzky-golay digital differentiator in digital image correlation. *Opt Eng* 2007;46(3). doi:10.1117/1.2714926.
- Malesa M, Kujawinska M, Malowany K, Lusa T. Application of multi-camera dic system for measurements of industrial structures. *Procedia Eng* 2015;114:453–60. doi:10.1016/j.proeng.2015.08.092.
- Tomasz R, Magdalena K. Characterization of biocompatible materials using stereo microscope 3d digital image correlation. *Adv Eng Mater* 18(9):1651–1660. <https://onlinelibrary.wiley.com/doi/pdf/10.1002/adem.201600266>; URL <https://onlinelibrary.wiley.com/doi/abs/10.1002/adem.20160026610.1002/adem.201600266>.